

Electronic Supplementary Information

**Photoresponsivity and antibiotic sensing properties of an entangled
tris(pyridinium)-based metal-organic framework**

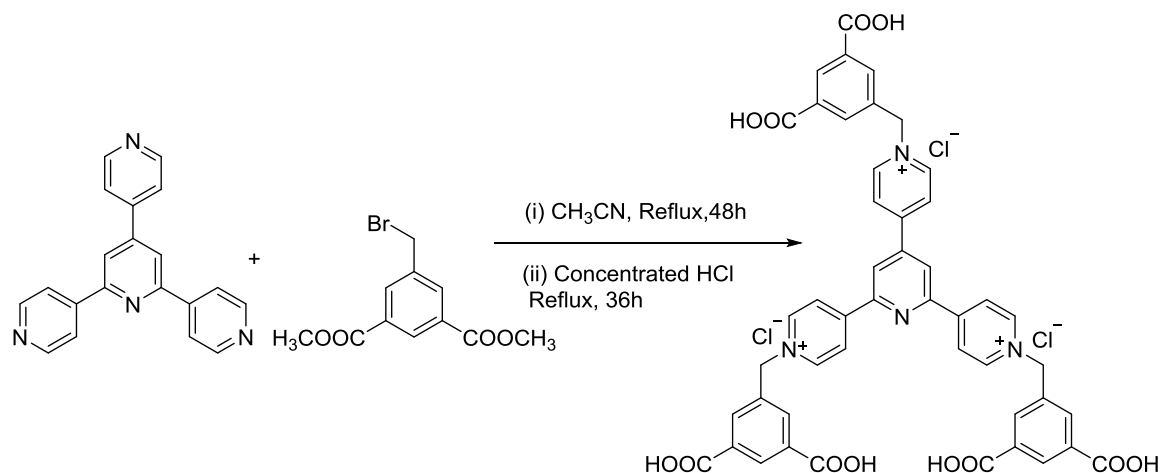
Peng Li,^a Meng-Yue Guo,^b Lu-Lu Gao,^a Xue-Mei Yin,^a Shuai-Liang Yang,^a Ran Bu,^a En-Qing Gao^{*a}

^aShanghai Key Laboratory of Green Chemistry and Chemical Processes, School of Chemistry and
Molecular Engineering, East China Normal University, Shanghai 200062, China.

^bEngineering Research Center for Nanophotonics and Advanced Instrument, School of Physics and
Electronic Science, East China Normal University, Shanghai 200062, China.

*Email: eqgao@chem.ecnu.edu.cn

Synthesis. All of the starting materials and solvents were of reagent grade and used without further purification.



Scheme S1. Synthesis of the [H₆L]Cl₃ ligand.

[H₆L]Cl₃. The ligand was prepared according to Scheme S1. 2.0 mmol 2,4,6-tris(4-pyridyl)pyridine (0.62 g) and 7.0 mmol dimethyl 3-(bromomethyl)isophthalate (2.0 g) in 300 mL acetonitrile were refluxed for 48 h. After cooling, the yellow solid formed was collected by filtration, washed with CH₃CN, and then dried to give the ester precursor [Me₆L]Br₃. The ester was refluxed in concentrated HCl solution (50 mL) for 36 h. The pale yellow powder was filtrated, washed with water, and dried under vacuum. Yield: 54% base on 2,4,6-tris(4-pyridyl)pyridine. IR for [H₆L]Cl₃ (KBr, cm⁻¹): 1702 (m), 1641 (s), 1612 (m), 1571 (s), 1520 (m), 1446 (w), 1410 (m), 1365 (w), 1210 (m), 1161(w), 1135 (w), 1052 (w), 762 (s), 720 (w), 686 (m), 640 (w), 577 (w), 520 (w). The hexacarboxylic acid is hardly soluble in common solvents, which prevents us from obtaining its NMR spectrum. Therefore, we provide here the ¹H NMR data of the corresponding ester. ¹H NMR for [Me₆L]Br₃ (400 MHz, DMSO-d₆, δ/ppm): 9.67 (d, 2H, J = 6.4 Hz, pyridinium), 9.57 (d, 4H, J = 6.5 Hz, pyridinium), 9.26 (s, 2H, pyridyl), 9.25 (d, 4H, J = 6.5 Hz, pyridinium), 9.06 (d, 2H, J = 6.4 Hz, pyridinium), 8.58 (s, 2H, benzene), 8.56 (s, 4H, benzene), 8.52(s, 3H, benzene), 6.12 (s, 6H, CH₂). The IR and ¹H NMR spectra are provided in Fig. S1.

Physical Measurements. NMR spectra were recorded on a Bruker Advance 400 MHz spectrometer. Powder X-ray diffraction (PXRD) was recorded on a Rigaku D/Max-2500 diffractometer at 35 kV, 25 mA for a Cu-target tube and a graphite monochromator in a 2θ range of 5-40° at room temperature. UV-vis spectra were obtained on a SHIMADZU UV-2700 spectrometer. BaSO₄ plates were used as references (100% reflection), on which the finely ground power of a sample was coated. FT-IR spectra were recorded in the

range 500–4000 cm^{-1} using KBr pellets on a Nicolet NEXUS 670 spectrophotometer. Electron spin resonance (ESR) spectra were recorded on a Bruker Elexsys 580 spectrometer with a 100 kHz magnetic field in the X band at room temperature. Thermal gravimetric analysis (TGA) was performed on a STA 449 F3 Simultaneous Thermal Analyzer in flowing air at 10°C/min. Cyclic voltammetry (CV) experiments were carried out at room temperature in solution of ethanol with a CHI 604E electrochemical analyzer (Shanghai). All CV experiments were performed at a scan rate of 150 mV s^{-1} using a three-electrode system. A glassy carbon electrode (GCE) modified with the MOF or the ligand was used as the working electrode, a platinum wire as the counter electrode, and an Ag/AgCl electrode as the reference electrode, respectively. Electrochemical measurements were performed in aqueous solution with 0.1 M KCl as supporting electrolyte.

Preparation of antibiotic stock solutions. An antibiotic (5 mmol) was dissolved in a 20 mL solution of NaOH (0.01 M) under magnetic stirring. Deionized water was then added to a constant volume of 50 mL. The pH values of all antibiotic stock solutions are about 8 to 9.

Photochromic experiment. Photochromic tests were carried out using a 300W xenon lamp system (CEL-HXUV300, Ceaulight, China) equipped with an IR filter, and the samples was placed at 5 cm from the lamp. The solid-state UV-vis diffusive reflectance and fluorescence spectra were recorded using the same sample after irradiation for the given time.

Crystal structure determination. Data collection was performed using a Bruker Apex Smart Oxford Diffraction diffractometer (Cu- K_{α} radiation, $\lambda = 1.54184 \text{ \AA}$) equipped with a graphite monochromator and a CCD area detector. Structure solution was carried out using the direct method, and full-matrix least-squares refinements were performed on F^2 with the SHELX-2014 program. Non-hydrogen atoms were all refined anisotropically. The H atoms attached to carbons were added geometrically and refined isotropically with the riding model. The free solvent molecules of **1** were highly disordered, and no satisfactory disorder model could be achieved. Thus, the PLATON/SQUEEZE routine was used to remove their diffraction contributions. CCDC number: 1965214. Selected crystal data and structure refinement parameters are given in Table S1.

Table S1. Crystal data and structure refinement for **1**.

1	
Empirical formula	C ₄₇ H ₃₁ N ₄ O ₁₃ ClCd ₂
Formula weight	1120.01
Crystal system	monoclinic
Space group	<i>P</i> 2 ₁ / <i>n</i>
<i>a</i> , Å	9.8438(2)
<i>b</i> , Å	18.8552(3)
<i>c</i> , Å	28.4652(5)
α , deg	90
β , deg	93.1390(10)
γ , deg	90
<i>V</i> , Å ³	5275.41(16)
ρ calcd, g cm ⁻³	1.41
μ , mm ⁻¹	7.44
θ range collected	2.812 to 65.000
<i>S</i> on <i>F</i> ²	1.083
R ₁ [<i>I</i> > 2 σ (<i>I</i>)]	0.0754
wR ₂ (all data)	0.2108

Table S2. Comparison of **1** with recent MOF-based luminescent sensors for NFZ and NFT.

Fluorescent Materials	Analyte	K_{SV} (M^{-1})	DL (μM)	Medium	Ref.
[Cd ₃ (CBCD) ₂ (DMA) ₄ (H ₂ O) ₂]	NFZ	9.7×10^4	0.42	DMA	1
	NFT	6.4×10^4	0.53	DMA	
[Eu ₂ Na(Hpddb)(pddb) ₂ (CH ₃ COO) ₂]	NFZ	4.9×10^4	0.64	DMF	2
	NFT	4.4×10^4	0.68	DMF	
[Cd ₂ (L)(bpda) ₂]	NFZ	3.1×10^4	1.27	DMF	3
	NFT	2.2×10^4	1.95	DMF	
[Cd(tptc) _{0.5} (bimb)] _n	NFZ	4.4×10^4	0.21	DMF	4
	NFT	3.4×10^3	0.30	DMF	
[Cd(H ₂ tptc) _{0.5} (<i>m</i> -bimb)(Cl)] _n	NFZ	2.1×10^5	0.07	DMF	
	NFT	2.6×10^5	0.07	DMF	
[NaCd ₂ (L)(BDC)2.5]	NFZ	5.1×10^4	0.67	DMF	5
	NFT	3.5×10^4	1.10	DMF	
[Cd ₂ (L)(2,6-NDC) ₂]	NFZ	1.0×10^5	0.37	DMF	
	NFT	7.2×10^4	0.55	DMF	
[Cd ₂ (L)(BPDC) ₂]	NFZ	1.3×10^5	0.30	DMF	
	NFT	6.9×10^4	0.59	DMF	
RhB@[Me ₂ NH ₂][Tb ₃ (dcpcpt) ₃ (HCOO)]	NFZ	5.9×10^4	0.50	Water	6
	NFT	6.7×10^4	0.45	Water	
[Zn ₂ (Py ₂ TTz) ₂ (BDC) ₂]	NFZ	1.7×10^4	0.91	Water	7
[Cd ₂ (Py ₂ TTz) ₂ (BDC) ₂]	NFZ	4.5×10^4	0.85	Water	
[Tb(TCPB)(DMF)]	NFZ	3.1×10^4	0.13	Water	8
	NFT	2.4×10^4	0.18	Water	
[Zn ₄ O(BCTPE) ₃]	NFZ	NA	0.50	Water	9
Zr ₆ O ₄ (OH) ₈ (H ₂ O) ₄ (CTTA) _{8/3}	NFZ	1.1×10^5	0.29	Water	10
	NFT	3.8×10^4	0.38	Water	
Zr ₆ O ₄ (OH) ₈ (H ₂ O) ₄ (TTNA) _{8/3}	NFZ	7.5×10^4	NA	Water	
	NFT	6.0×10^4	NA	Water	
[TbZn ₃ (L) ₃ (HCOO)(H ₂ O) ₂]	NFZ	1.8×10^6	0.19	Water	11
	NFT	9.2×10^5	0.21	Water	
[Cd ₂ Cl(L)(H ₂ O)]	NFZ	2.1×10^4	0.20	Water	The work
	NFT	1.5×10^4	0.26	Water	

H₃CBCD= 4,4'-(9-(4'-carboxy-[1,1'-biphenyl]-4-yl)-9H-carbazole-3,6-diyl)dibenzoic acid.

pddb = 4,4'-(pyridine-2,6-diyl)dibenzolate.

L = 3,3',5,5'-tetra(1H-imidazol-1-yl)biphenyl, H₂bpda = 4,4'-carbonyldibenzoic acid.

H₄tptc = *p*-terphenyl-2,2'',5'',5'''-tetracarboxylate acid, bimb = bis(imidazol-1-ylmethyl)benzene.

L = (4-(1H-1,2,4-triazole-1-yl)benzyl)-N1-(2-aminoethyl)ethane-1,2-diamine.

H₃dcpcpt = 3-(3,5-dicarboxylphenyl)-5-(4-carboxylphenyl)-1H-1,2,4-triazole.

Py₂TTz = 2,5-bis(4-pyridyl)thiazolo[5,4-d]thiazole, BDC = 1,4-benzenedicarboxylate.

H₃TCPB = 3,5-tris(4-carbonylphenoxy)benzene.

H₂BCTPE = 4,4'-(1,2-diphenylethene-1,2-diyl)dibenzoic acid.

H₃CTTA = 5'-(4-carboxyphenyl)-2',4',6'-trimethyl-[1,1':3',1''-terphenyl]-4,4''-dicarboxylic acid,

H₃TTNA = 6,6',6''(2,4,6-trimethylbenzene-1,3,5-triyl)tris(2-naphthoic acid).

H₃L = 4-(2,4,6-tricarboxyl phenyl)-2,2':6',2''-terpyridine.

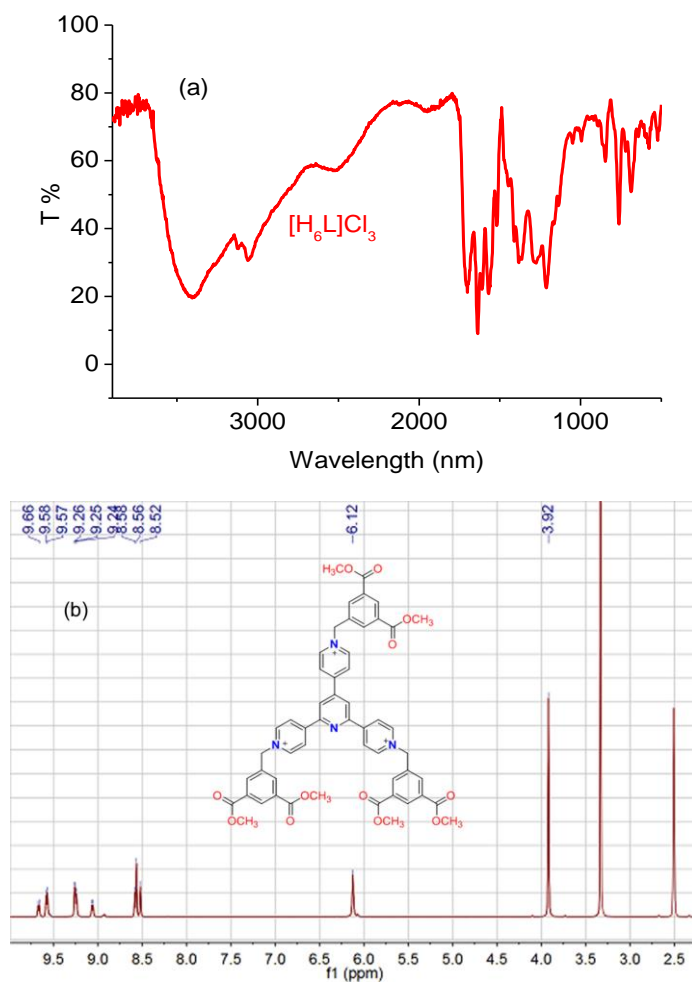


Fig. S1 (a) IR spectrum of $[H_6L]Cl_3$. (b) 1H NMR spectrum of $[Me_6L]Br_3$.

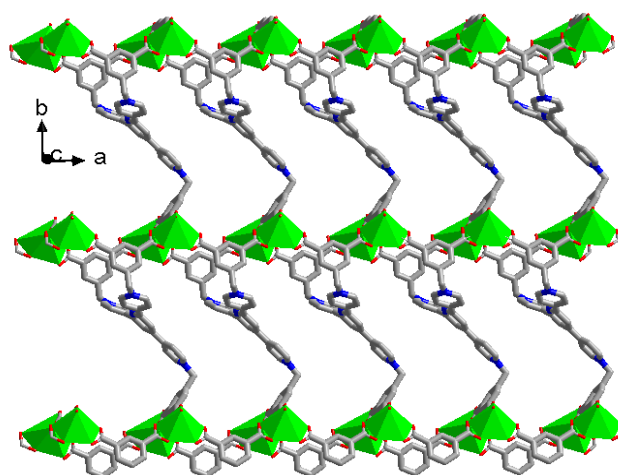


Fig. S2 View of the 2D layer along ab plane.

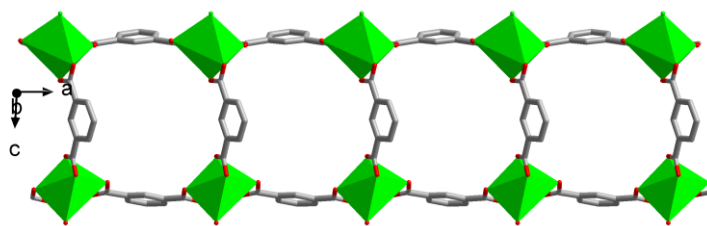


Fig. S3 The ladder-like chain along *a* axis.

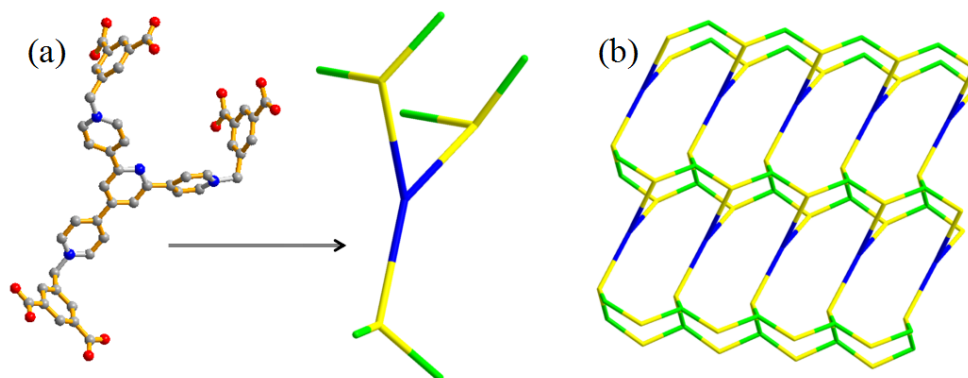


Fig S4 Topological representations of the ligand(a) and the structure of **1** (b).

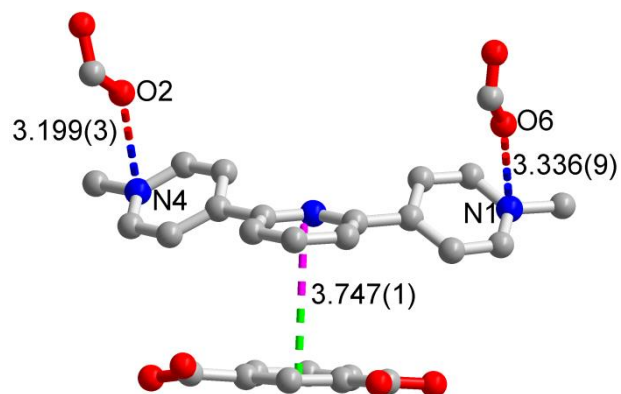


Fig S5 The π - π stacking and n - π interactions in **1**. The distances are given in Å.

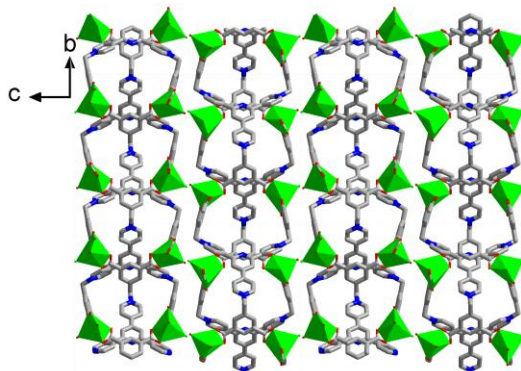


Fig. S6 Packing of the 2D bilayers in **1**.

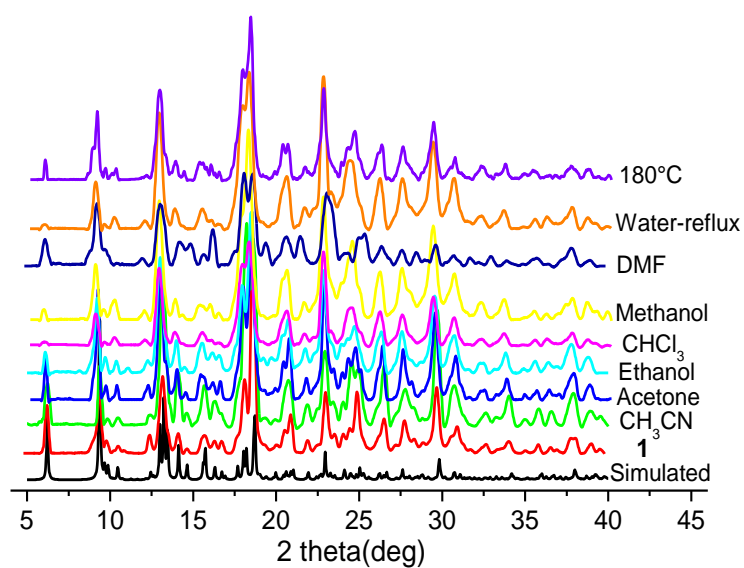


Fig. S7 PXRD patterns of **1** after soaking in different solvents and heating at 180°C (1 h).

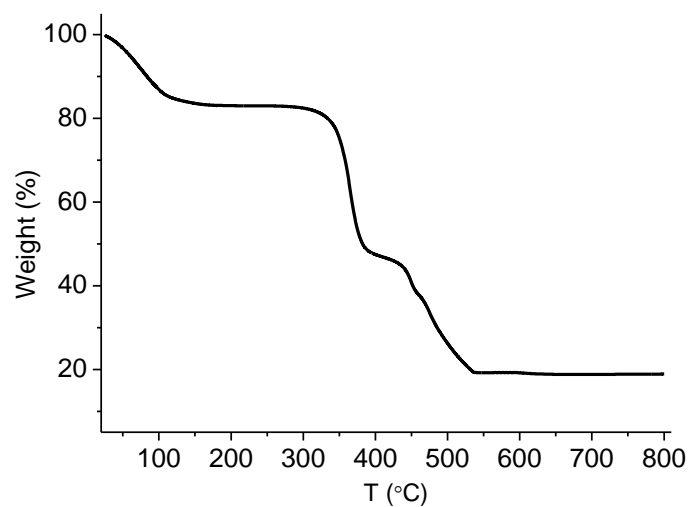


Fig. S8 TGA curve of **1**.

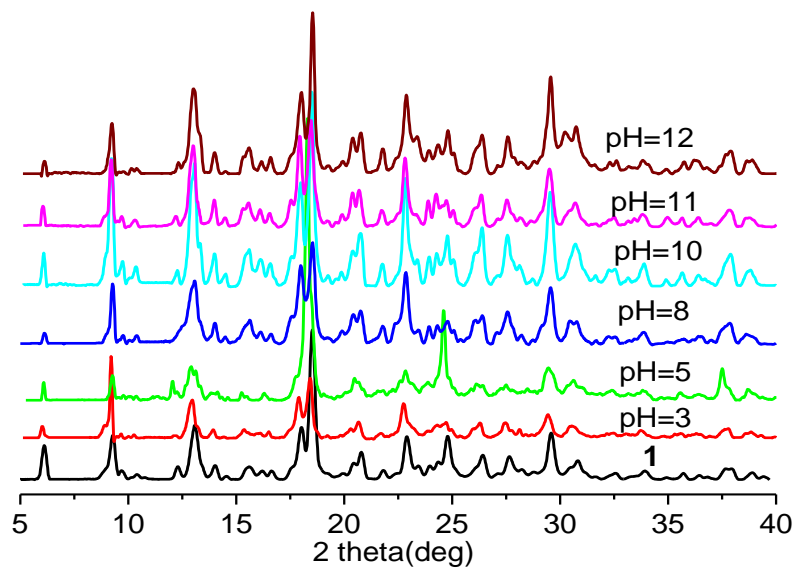


Fig. S9 PXR D patterns of **1** after soaking in aqueous solutions with different pH values.

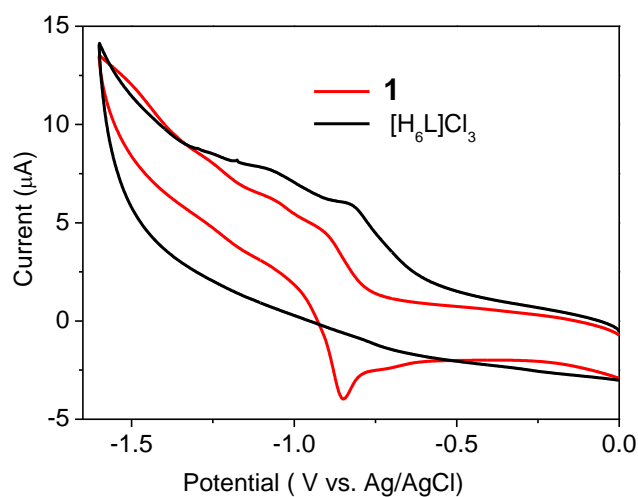


Fig. S10 Cyclic voltammograms of $[H_6L]Cl_3$ and **1** (0.1 M KCl solution, scan rate $150 \text{ mV} \cdot \text{s}^{-1}$).

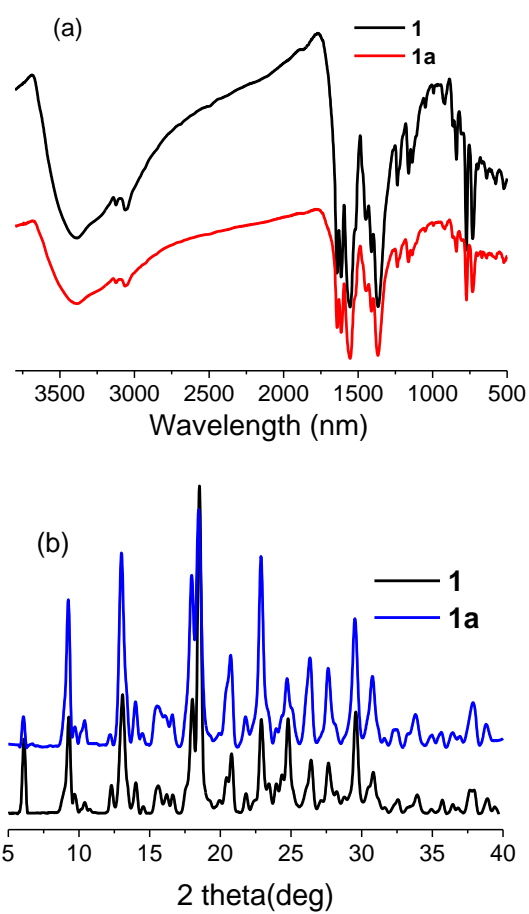


Fig. S11 (a) IR spectra and PXRD patterns (b) of the MOF before (**1**) and after (**1a**) irradiation.

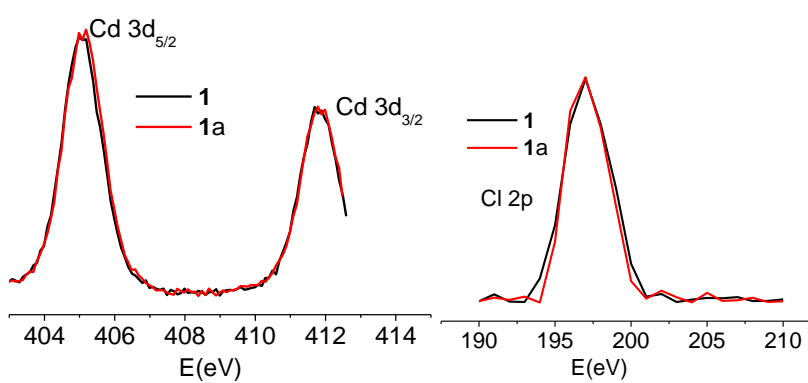


Fig. S12 XPS core-level spectra of the MOF before (**1**) and after (**1a**) irradiation.

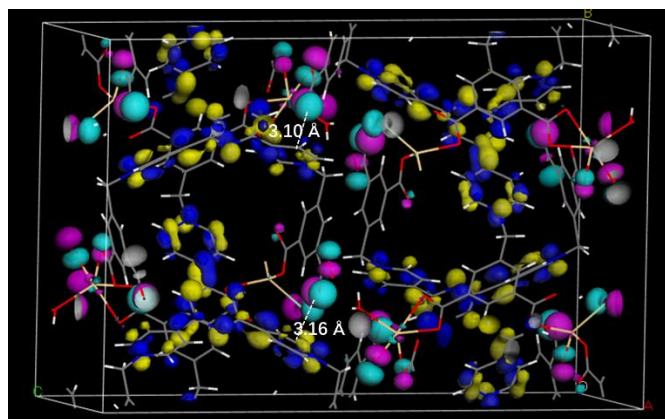


Fig. S13 3D isosurfaces of selected highest occupied molecular orbitals (HOMOs, purple and cyan) and lowest unoccupied molecular orbitals (LUMOs, blue and yellow) of **1**. The distances from the carboxylate oxygens to the of the pyridinium rings are marked. The orbital calculations were performed using the DMol³ module in the Materials Studio software package.¹²⁻¹⁴ The PW91 local functional and the DNP 4.4 basis set were adopted. The calculations were based on the single-crystal structure in which the disordered atoms were set at the average positions.

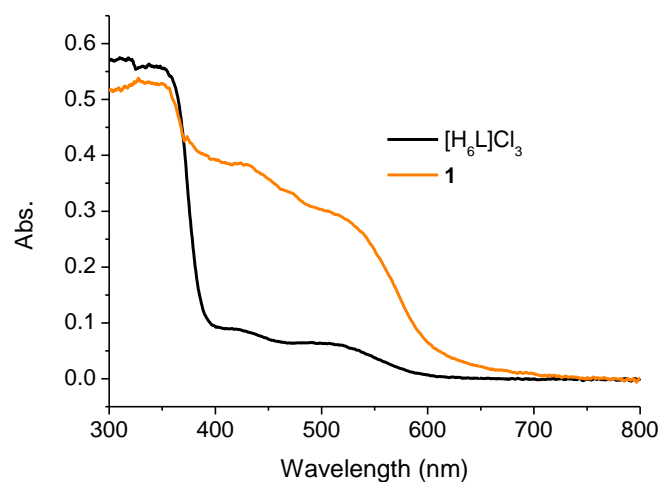


Fig. S14 Solid-state UV-vis absorption spectra of **1** and the ligand.

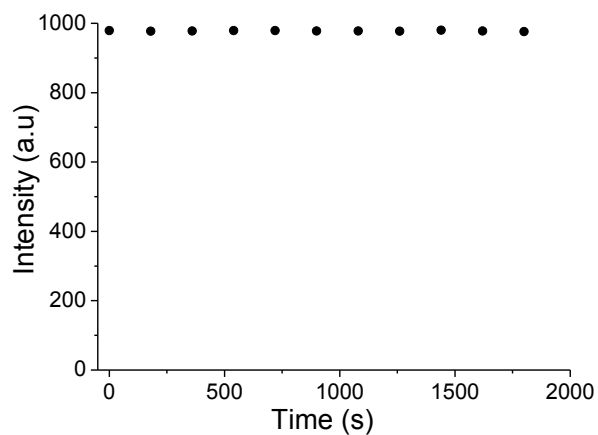


Fig. S15 A kinetic measurement of the emission intensity (at 420 nm) of the aqueous suspension of **1**.

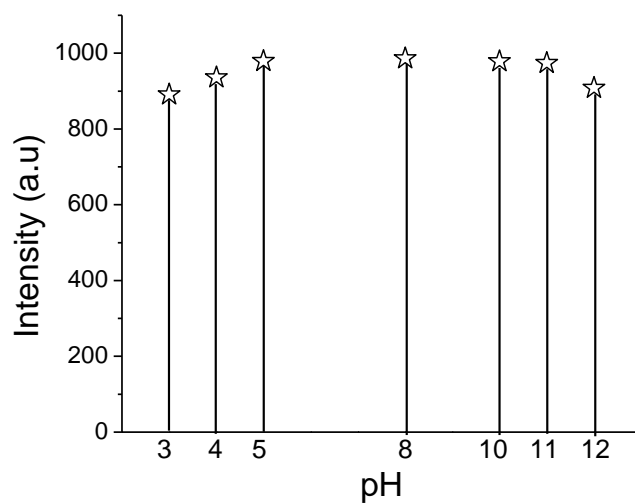


Fig. S16 Emission intensity (at 420 nm) of the aqueous suspensions of **1** at different pH.

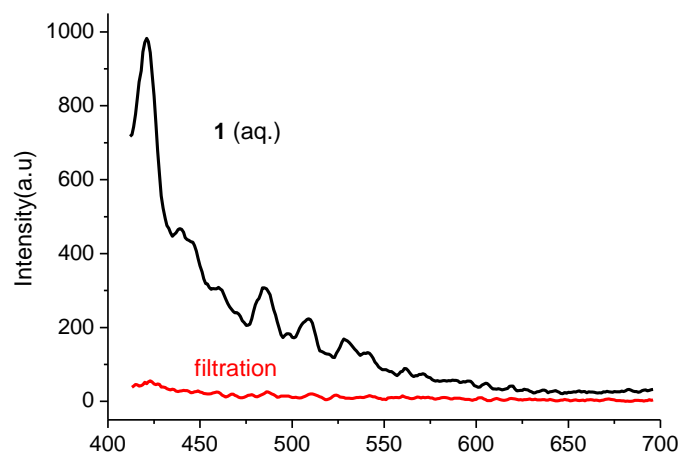


Fig. S17 Comparison of the emission spectra of the aqueous suspension of **1** and the supernatant after filtration.

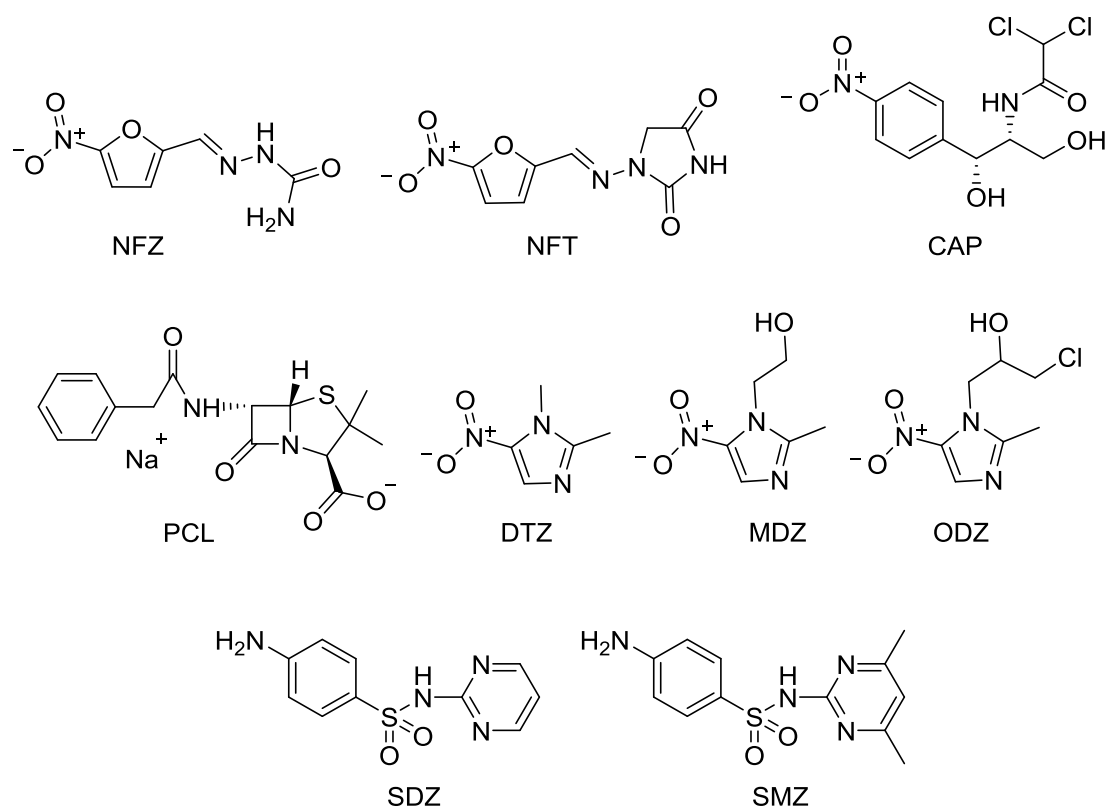


Fig. S18 Chemical structures of selected antibiotics.

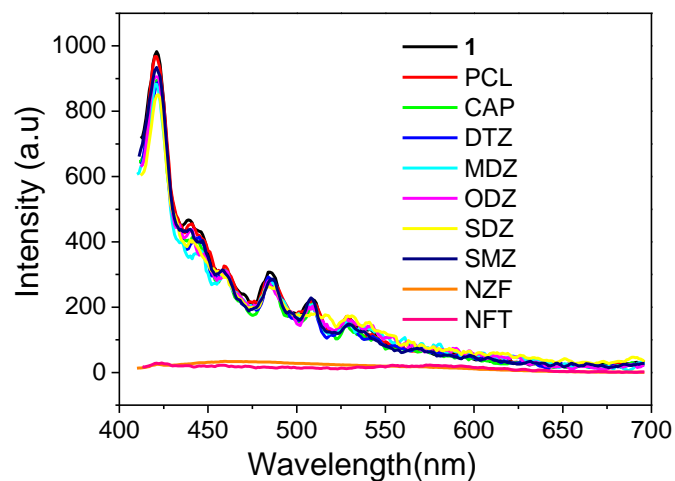


Fig. S19 Emission spectra of the aqueous suspensions of **1** before and after addition of various antibiotics (1.0 mM).

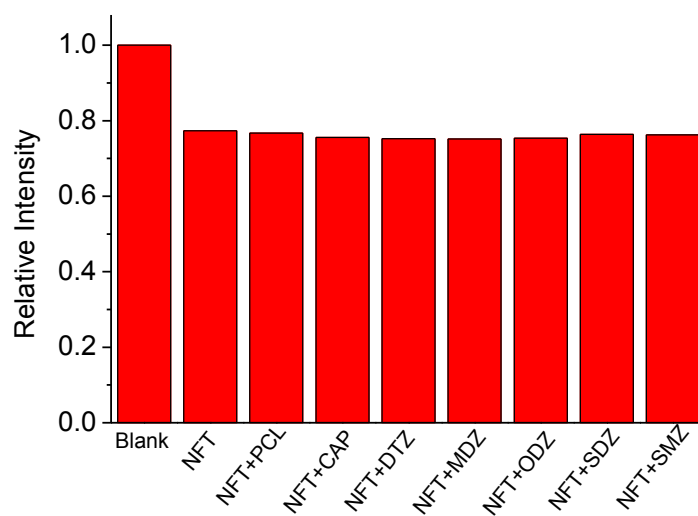


Fig. S20 The response of the dispersion of **1** to 0.02 mM NFT in absence and presence of excessive antibiotics of other classes (0.10 mM).

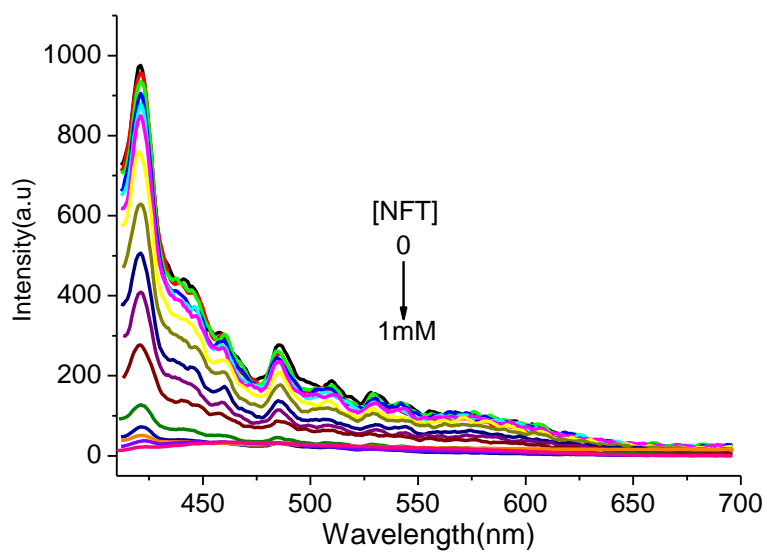


Fig. S21 Variation of the emission spectra of **1** with the incremental concentrations of NFT.

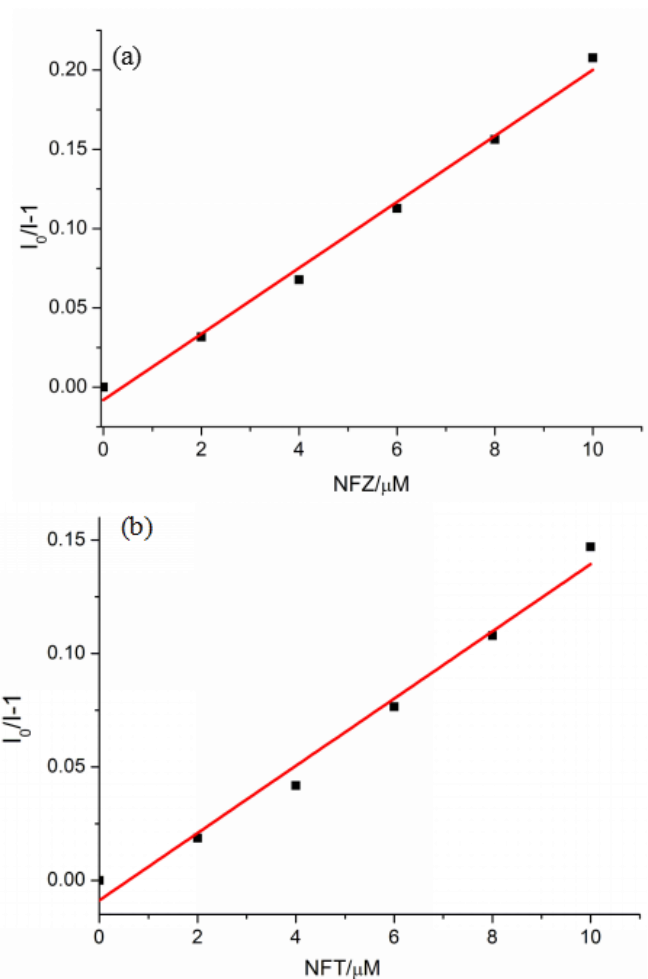


Fig. S22 Linear regression of the SV plots for NFZ (a) and NFT (b) in low concentration ranges.

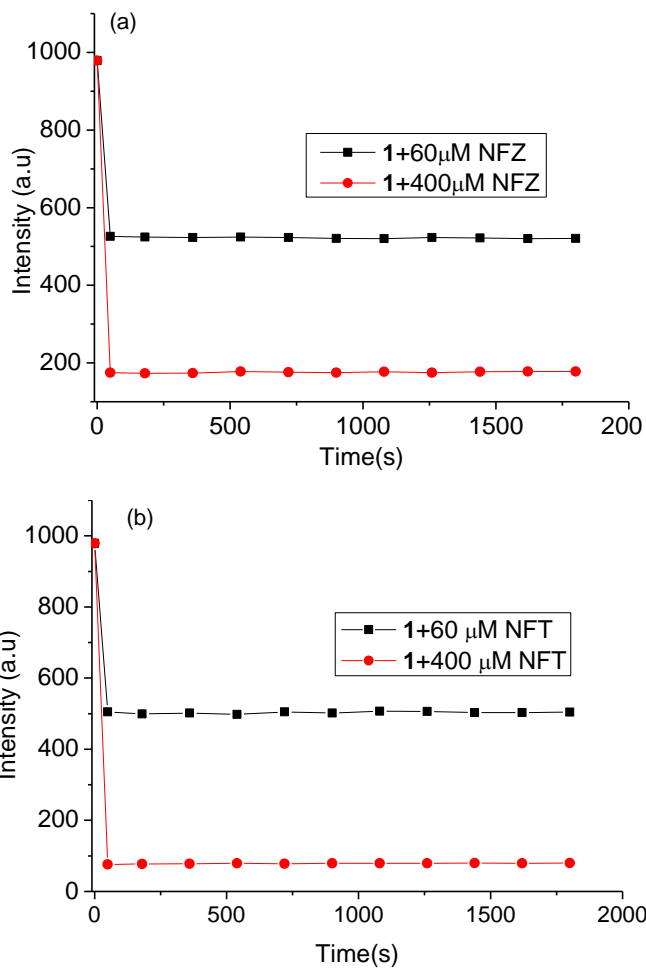


Fig. S23 Kinetic measurements of the emission intensity at 420 nm after adding NFZ (a) and NFT (b) to the aqueous suspensions of **1**.

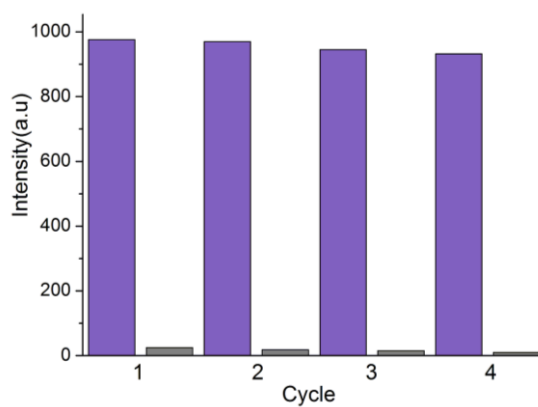


Fig. S24 Relative emission intensity (420 nm) of the aqueous dispersions of original and regenerated samples of **1** (four cycles) before (violet) and after (gray) the addition of NFT (1 mM)..

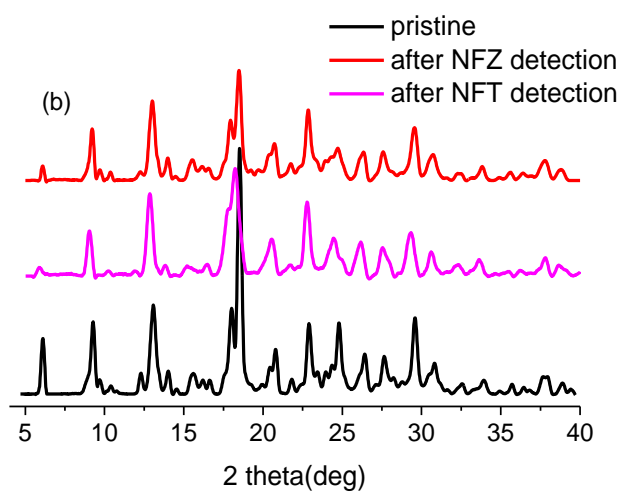
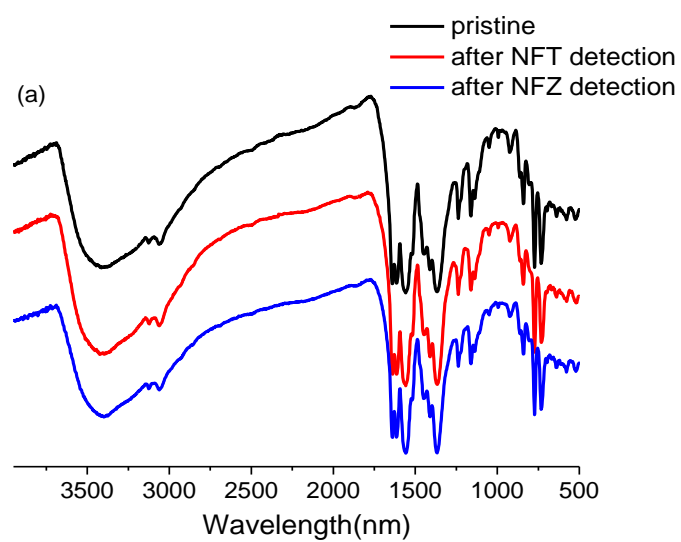


Fig. S25 The IR spectra (a) and PXRD (b) patterns of **1** before and after detection of NFZ or NFT.

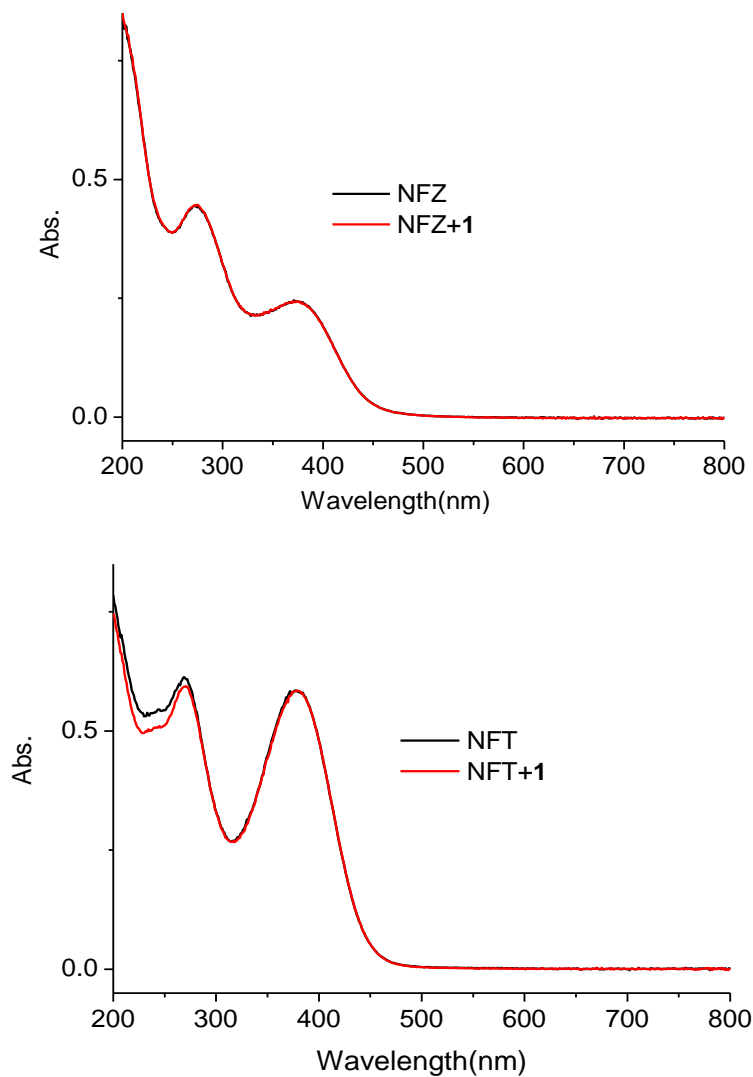


Fig. S26 The UV-vis absorption spectra of NFZ or NFT (0.005 M) before and after adding an excessive amount of **1** (0.015 M).

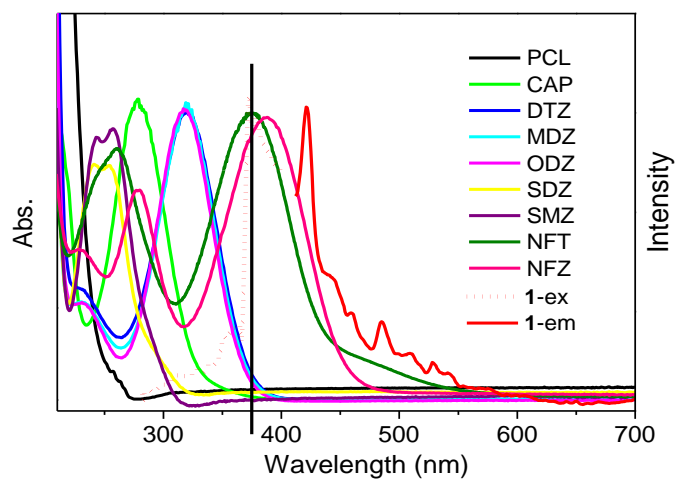


Fig. S27 The UV-vis absorption spectra of the antibiotics and the excitation and emission spectra of **1**.

Reference

1. N. Xu, Q. Zhang and G-A Zhang. *Dalton Trans.*, 2019, **48**, 2683.
2. S. Xu, J.-J. Shi, B. Ding, Z.-Y. Liu, X.-G. Wang, X.-J. Zhao and E.-C. Yang, *Dalton Trans.*, 2019, **48**, 1823.
3. Y.-L. Xu, Y. Liu, X.-H. Liu, Y. Zhao, P. Wang, Z.-L. Wang and W.-Y. Sun. *Polyhedron*. 2018, **154**, 350.
4. Y. Zhang, J. Yang, D. Zhao, Z. Liu, D. Li, L. Fan and T. Hu. *CrystEngComm.*, 2019, **21**, 6130-6135.
5. D. Zhao, X.-H. Liu, Y. Zhao, P. Wang, Y. Liu, M. Azam, S. I. Al-Resayes, Y. Lu and W.-Y. Sun. *J. Mate. Chem A.*, 2017, **5**, 15797.
6. M. Yu, Y. Xie, X. Wang, Y. Li and G. Li. *ACS Appl. Mater. Interfaces.*, 2019, **11**, 21201.
7. Z.-W. Zhai, S.-H. Yang, M. Cao, L.-K. Li, C. Du and S.-Q. Zang. *Cryst. Growth Des.*, 2018, **18**, 7173.
8. J. Zhang, L. Gao, Y. Wang, L. Zhai, X. Niu and T. Hu. *CrystEngComm.*, 2019, **21**, 7286.
9. X.-G. Liu, C.-L. Tao, H.-Q. Yu, B. Chen, Z. Liu, G.-P. Zhu, Z. Zhao, L. Shen and B.-Z. Tang. *J. Mate. Chem C.*, 2018, **6**, 2983.
10. B. Wang, X.-L. Lv, D. Feng, L.-H. Xie, J. Zhang, M. Li, Y. Xie, J.-R. Li and H.-C. Zhou. *J. Am. Chem. Soc.*, 2016, **138**, 6204.
11. Q.-Q. Zhu, H. He, Y. Yan, J. Yuan, D.-Q. Lu, D.-Y. Zhang, F. Sun and G. Zhu. *Inorg. Chem.*, 2019, **58**, 7746.
12. B. Delley, *J. Chem. Phys.*, 1990, **92**, 508.
13. B. Delley, *J. Chem. Phys.*, 2000, **113**, 7756.
14. Materials Studio. version 6.0. Accelrys Software Inc.: San Diego, CA, **2010**.